Full Length Article

The role of Co/Al ratio in glass-forming GdCoAl magnetocaloric metallic glasses

Liliang Shao [a,1], Lin Xue [a,1], Qiang Luo [a], Qianqian Wang [a], Baolong Shen [a,b,*]

[a] School of Materials Science and Engineering, Jiangsu Key Laboratory of Advanced Metallic Materials, Southeast University, Nanjing 211189, China
[b] Institute of Massive Amorphous Metal Science, China University of Mining and Technology, Xuzhou 221116, China

ABSTRACT

In this work, a prominent improvement of glass-forming ability is achieved through the adjustment of Co/Al ratio in the ternary GdCoAl system. The critical diameter of $Gd_{55}Co_{17.5}Al_{27.5}$ bulk metallic glass (BMG) is up to 8 mm, which is larger than that of the $Gd_{55}Co_{22.5}Al_{22.5}$ BMG with a critical diameter of 3 mm and most ternary Gd-based BMGs. Thermodynamic investigations in terms of specific heat capacity and Gibbs free energy difference indicate that the $Gd_{55}Co_{17.5}Al_{27.5}$ BMG possesses a lower driving force for crystallization. Kinetic analyses based on viscosity and dynamic relaxation spectrum reveal a stronger liquid behavior and more sluggish kinetics of the $Gd_{55}Co_{17.5}Al_{27.5}$ BMG compared with the $Gd_{55}Co_{22.5}Al_{22.5}$ BMG. Through the combination of the linear thermal expansion behavior and relaxation, the distinct difference of the contraction in supercooled liquid region of $Gd_{55}Co_{17.5}Al_{27.5}$ and $Gd_{55}Co_{22.5}Al_{22.5}$ BMGs is well explained. In addition, the magnetic entropy change is further enhanced by appropriate annealing treatment through the formation of more complex structures comprising short-range order, medium-range order and nano-crystallized structure.

1. Introduction

Rare earth (RE)-based metallic glasses (MGs) with a wide range of tunable compositions exhibit excellent functional and abundant physical properties [1–5], such as magnetocaloric effect (MCE) which is the basis of magnetic refrigeration technology [6,7]. Compared with conventional refrigeration technologies, the magnetic refrigeration has advantages of high refrigeration efficiency, wide category of refrigerants and environmental friendliness [8–10]. Crystalline materials may exhibit giant magnetic entropy change (ΔS_M) attributed to the first-order structural transition coupled with the ferromagnetic (FM) to paramagnetic (PM) transition. However, magnetic and heat hysteresis for crystalline refrigerants is unneglectable and their refrigerant capacity (RC) is inadequate [11–13]. In contrast, relatively large $|\Delta S_M|$ and broad full width at half maximum of $|\Delta S_M|$ (δT_{FWHM}) are usually available in MGs due to the intrinsic amorphous structure and second-order magnetic transition [1].

In particular, Gd-based MGs have attracted tremendous research interests due to their remarkable MCE manifested as negligible magnetic hysteresis and broad phase transition temperature range. In the past decade, a serious of Gd-based MGs in the forms of microwire, ribbon, and rod with good MCE have been investigated [14–17]. Among them,

the most widely studied alloy system is GdTMAl (TM = Fe, Co, Ni), and excellent RC was obtained in considerable compositions [18–21], furthermore, table-like MCE was achieved in several systems through inducing appropriate crystalline phases [22,23]. Through the substitution of similar RE elements, the controllable spin glass-like behavior and magnetocaloric response can be realized in GdRETMAl (RE = Tb, Dy, Ho, Er, Tm, TM = Co, Fe, Ni) MGs [24–27]. Besides, binary Gd-based MGs such as GdCo, GdNi ribbons have also been studied to some extent [28,29]. However, the critical diameters of these Gd-based magnetic MGs were usually less than 3 mm, and the wide application was tremendously limited by the inadequate glass-forming ability (GFA). Although some works have been devoted to the improvement of the GFA of Gd-based bulk metallic glasses (BMGs), such as microalloying [30], substitution with similar RE elements [15], and utilization of high entropy alloy characteristics [31,32], etc., the effects are usually not significant or could result in the deterioration of RC. Generally, large GFA corresponds to high thermal stability and guarantees the process of all kinds of complex structures, which can make contribution to the practical application of amorphous magnetic refrigerants. Therefore, simultaneously achieving the enhancement of GFA and preservation of excellent MCE for Gd-based MGs through delicate composition adjustment is of great significance.

---

* Corresponding author at: School of Materials Science and Engineering, Jiangsu Key Laboratory of Advanced Metallic Materials, Southeast University, Nanjing 211189, China.
E-mail address: blshen@seu.edu.cn (B. Shen).
[1] These authors contribute equally to this work.

In addition, most investigations on the GFA of Gd-based MGs are still at the stage of composition exploration, and the detailed and systematic study of GFA and thermophysical characterization remain insufficient. In contrast, more and more BMGs such as Zr-, Fe-, Ni-, Pt-, Pd- and Mg-based alloy systems were deeply studied with respect to thermodynamic and kinetic aspects recently [33–40], identifying the close correlation between GFA and thermophysical properties including specific heat capacity (c_p), Gibbs free energy difference, viscosity and fragility, etc. Consequently, the exploration of the thermophysical properties for Gd-based BMGs will contribute to the intensive investigation of GFA for RE-based MGs, which can provide theoretical guidance for the development of new materials with advanced functional performance.

In order to achieve the combination of large GFA and prominent MCE in Gd-based MGs, ternary GdCoAl BMGs with different Co/Al ratios are prepared. The critical diameter of the $Gd_{55}Co_{17.5}Al_{27.5}$ BMG is up to 8 mm, which is the largest in ternary Gd-based BMGs up to now. Furthermore, the correlation between the enhanced GFA and thermophysical properties are systematically investigated from thermodynamic and kinetic aspects. The linear thermal expansion and relaxation behaviors of $Gd_{55}Co_{17.5}Al_{27.5}$ and $Gd_{55}Co_{22.5}Al_{22.5}$ BMGs are also studied in order to better understand the distinct difference on GFA. Due to the preservation of high Gd content, excellent MCE is obtained in both alloys. The ΔS_M is further enhanced by reasonable annealing treatment through introducing appropriate portion of medium-range order (MRO) and nano-crystallized (NC) structure into the amorphous matrix, which is of great significance to tailor MCE.

2. Experimental

Pre-alloyed ingots with nominal compositions of $Gd_{55}Co_{22.5}Al_{22.5}$ and $Gd_{55}Co_{17.5}Al_{27.5}$ were prepared by arc melting a mixture of Gd, Co, Al under highly pure argon atmosphere. The purity of raw materials used in this study is beyond 99.9%. In order to achieve chemical homogeneity, all of the ingots were re-melted for five times. Subsequently, BMGs with diameters of 1–8 mm were prepared by copper mold casting method under argon atmosphere.

The microstructures of BMGs were investigated by X-ray diffraction (XRD, Bruker D8) with Cu Kα radiation, and high-resolution transmission electron microscopy (HRTEM, Tecnai G20, FEI). Thermal analysis was carried out by differential scanning calorimeter (DSC, Netzsch DSC 404 F3) using the BMG with diameter of 2 mm under high-purity argon flow. Characteristic temperatures like the glass transition temperature (T_g), the crystallization temperature (T_x) and the melting point (T_m) of samples were obtained from the corresponding DSC curves. Three kinds of thermal analyses, i.e., isochronal annealing below T_g, isothermal annealing between T_g and T_x and heating with various heating rates of 5, 10, 20, 30, 40 and 50 K/min were applied to characterize the thermal properties of BMGs. The process of isochronal annealing was set as (1) heated the sample to a pre-set temperature below T_g with a heating rate of 20 K/min and held for 60 min, (2) cooled the sample to room temperature (RT), (3) heated the preprocessed sample from RT to 883 K with a heating rate of 20 K/min. In parallel, the amorphous sample was isothermally annealed at several temperatures between T_g and T_x for a certain time depending on the crystallization behavior. The temperature step method was selected to obtain the stable value of c_p in order to overcome the influence of the reproducibility of the DSC baseline [36]. The samples were heated at a constant rate of 20 K/min to a certain temperature with series of temperature intervals of 10 K and holding isothermally for 10 min. The value of c_p was obtained from the following formula:

$$c_p(T)_{sample} = \frac{\dot{Q}_{sample} - \dot{Q}_{pan}}{\dot{Q}_{sapphire} - \dot{Q}_{pan}} \times \frac{m_{sapphire} \times \mu_{sample}}{m_{sample} \times \mu_{sapphire}} \times c_p(T)_{sapphire} \qquad (1)$$

where $\dot{Q}$, m and μ refer to heat flow, mass and molar mass, respectively.

A thermomechanical analyzer (TMA, Netzsch TMA 402 F3) was used to obtain the kinetic viscosity in the vicinity of T_g and linear thermal ex-

pansion coefficient by dilatometry. Glassy rods with a diameter of 2 mm, a length of 10 mm or 3 mm and two plane parallel surfaces were heated from RT to 903 K with a constant heating rate of 10 K/min, during which a force of 0.2 N was applied. Subsequently, the dynamic viscosity η can be obtained: $\eta = \sigma/3\dot{\varepsilon}$ [41].

The dynamical mechanical spectroscopy of the MGs was performed on a dynamical mechanical analyzer (DMA, Netzsch DMA 242 E) in a high-purity nitrogen atmosphere. The dynamic modulus $E^*(\omega) = E'(\omega) + iE''(\omega)$, which includes a real part E' and an imaginary part E'' representing the storage and loss modulus, respectively. The beam-shaped specimens with the dimension of 30 mm × 2 mm × 1.5 mm were measured by single cantilever bending mode with a constant heating rate of 2 K/min at various frequencies of 0.2, 0.5, 1 and 2 Hz.

The temperature and field dependences of magnetization curves were measured by a SQUID magnetometer (MPMS, Quantum Design) using glassy rods with a diameter of 1 mm. The field cooling magnetization (M_{FC}) curve was measured under an applied magnetic field of 100 Oe on the heating course after initially cooling the sample from 300 to 2 K under the same field. The zero field cooling magnetization (M_{ZFC}) curve was measured on the heating course under the same field of M_{FC} after initially cooling from 300 to 2 K without applied magnetic field. The isothermal magnetization (M–H) curves were measured under a changing magnetic field up to 5 T, and the temperature varied from 2 to 200 K with an interval of 5 K near the magnetic transition temperature.

3. Results

3.1. Glass-forming ability

Fig. 1 shows XRD patterns and typical DSC traces of the as-cast $Gd_{55}Co_{17.5}Al_{27.5}$ and $Gd_{55}Co_{22.5}Al_{22.5}$ rods. Only broad hump in the 2θ range of 30°–40° can be seen for $Gd_{55}Co_{22.5}Al_{22.5}$ (diameter: 3 mm) and $Gd_{55}Co_{17.5}Al_{27.5}$ (diameter: 8 mm) rods, illustrating a fully amorphous structure. It is worth noting that the critical diameter of the $Gd_{55}Co_{17.5}Al_{27.5}$ BMG is the largest among the ternary GdCoAl BMGs reported up to date. As a contrast, the critical diameter of $Gd_{55}Co_{22.5}Al_{22.5}$ is only 3 mm. The inset picture of Fig. 1 exhibits the metallic lustrous surface of $Gd_{55}Co_{17.5}Al_{27.5}$ BMG with a diameter of 8 mm, indicating its excellent castability upon solidification. It can be seen from the DSC traces that both alloys exhibit a distinct broad endothermic hump corresponding to glass transition and subsequent exothermic peaks related to crys-
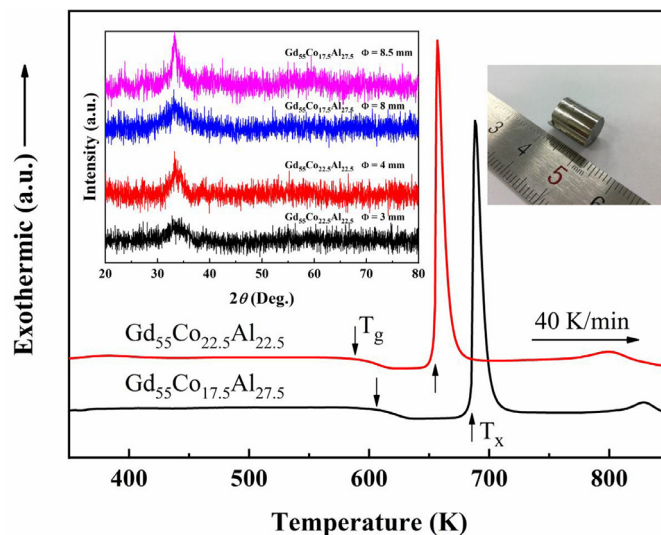

Fig. 1. XRD patterns and DSC traces of the as-cast $Gd_{55}Co_{17.5}Al_{27.5}$ and $Gd_{55}Co_{22.5}Al_{22.5}$ rods with diameter of 3–8.5 mm. Inset of this figure shows the picture of the $Gd_{55}Co_{17.5}Al_{27.5}$ BMG with a diameter of 8 mm.
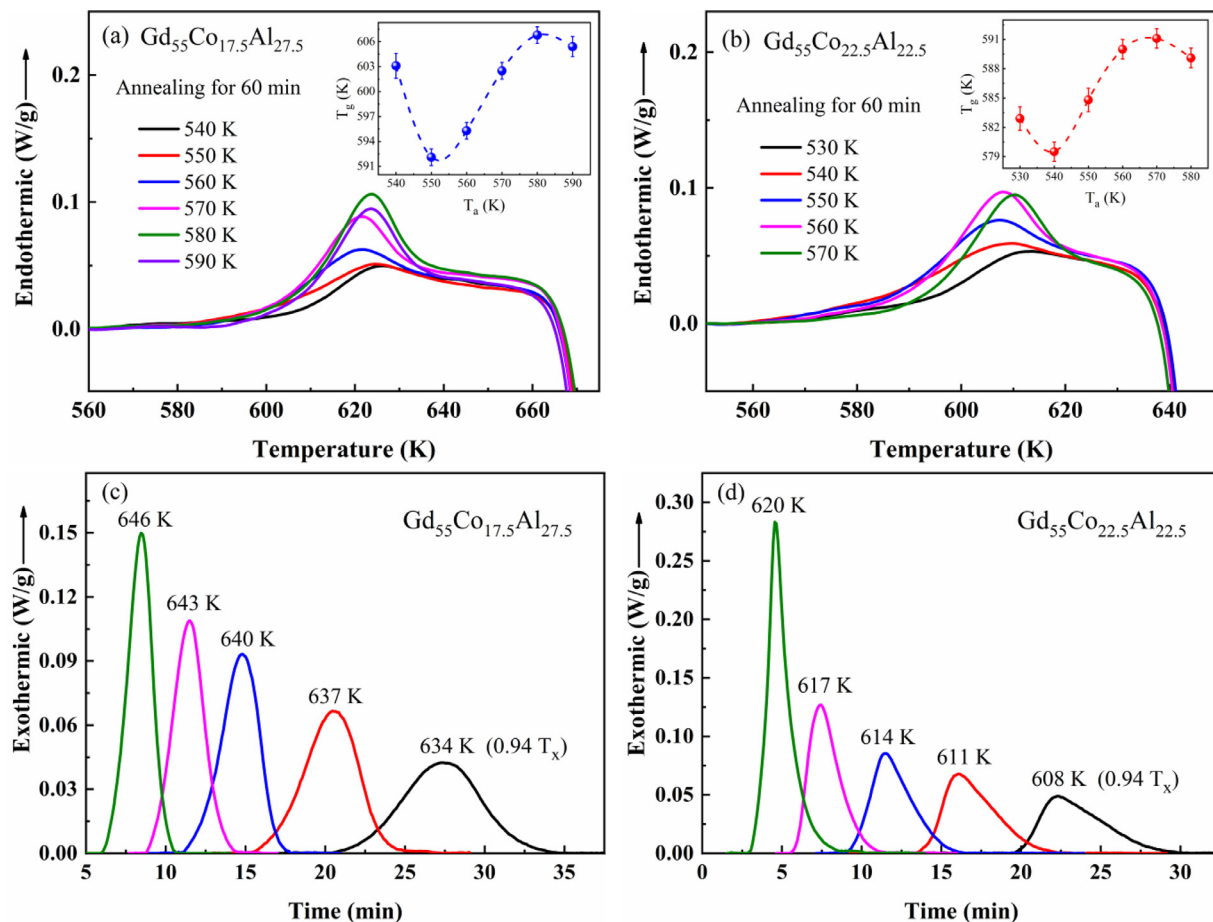
Fig. 2. DSC traces of the $Gd_{55}Co_{17.5}Al_{27.5}$ (a) and $Gd_{55}Co_{22.5}Al_{22.5}$ (b) BMGs annealed below T_g, and the insets show the relationship between T_g and T_a. Isothermal crystallization DSC curves with temperature interval of 3 K from 0.94 T_x for $Gd_{55}Co_{17.5}Al_{27.5}$ (c) and $Gd_{55}Co_{22.5}Al_{22.5}$ (d) BMGs.

Table 1
Thermodynamic and kinetic parameters for the glass formers of this study. a, b, c, d are the fitting parameters for c_p. D^* and T_0 are the fitting parameters of the VFT equation. m is the fragility index obtained from the DMA data.

Composition	$a \times 10^{-3}$ (J g-atom^{-1} K^{-2})	$b \times 10^6$ (J K g-atom^{-1})	$c \times 10^{-3}$ (J g-atom^{-1} K^{-2})	$d \times 10^{-5}$ (J g-atom^{-1} K^{-3})	D^*	T_0 (K)	m
$Gd_{55}Co_{17.5}Al_{27.5}$	7.85 ± 0.46	7.735 ± 0.264	9.91 ± 0.92	2.134 ± 0.154	28.2 ± 0.2	351.1 ± 0.6	36.7 ± 1.9
$Gd_{55}Co_{22.5}Al_{22.5}$	10.69 ± 0.42	6.865 ± 0.279	-12.14 ± 1.21	2.666 ± 0.201	20.6 ± 0.1	383.8 ± 0.5	44.2 ± 2.0

tallization. The supercooled liquid regions ΔT_x ($\Delta T_x = T_x - T_g$) are 80 and 65 K for $Gd_{55}Co_{17.5}Al_{27.5}$ and $Gd_{55}Co_{22.5}Al_{22.5}$, respectively, implying a more stable supercooled liquid and better GFA of the $Gd_{55}Co_{17.5}Al_{27.5}$ alloy.

3.2. Isochronal and isothermal annealing

In order to explicate the significant difference of the GFA of these similar glass formers, annealing treatments were selected. Fig. 2(a) shows the DSC traces of the $Gd_{55}Co_{17.5}Al_{27.5}$ BMG after isochronal annealing at different temperatures from 540 (0.9 T_g) to 590 K (0.983 T_g). The relationship between T_g and annealing temperature (T_a) is nonlinear as shown in the inset of Fig. 2(a), which implies that the kinetic stability of BMGs does not monotonically increase with the increase of T_a. The corresponding DSC traces of the $Gd_{55}Co_{22.5}Al_{22.5}$ BMG obtained from 530 (0.9 T_g) to 570 K (0.969 T_g) are shown in Fig. 2(b), which exhibit the similar variation trend with the $Gd_{55}Co_{17.5}Al_{27.5}$ BMG. Hu et al. found that the dependence of T_g on T_a is nonlinear when T_a is well below T_g [42]. The similar phenomenon is observed in this study at the vicinity of T_g. Furthermore, it is found that T_x keeps almost the same value within the experimental error below a critical temperature

(T_{ct}, 590 K for $Gd_{55}Co_{17.5}Al_{27.5}$, 570 K for $Gd_{55}Co_{22.5}Al_{22.5}$), above which T_x decreases slightly. It is confirmed that this slight difference is not caused by experimental errors and can be validated by the subsequent analysis. The T_{ct} of $Gd_{55}Co_{22.5}Al_{22.5}$ (0.969 T_g) is lower than that of $Gd_{55}Co_{17.5}Al_{27.5}$ (0.983 T_g), which is concordant with their different thermal stability. The crystallization kinetics of the $Gd_{55}Co_{17.5}Al_{27.5}$ and $Gd_{55}Co_{22.5}Al_{22.5}$ BMGs was studied by isothermal annealing at various temperatures between T_g and T_x as shown in Fig. 2(c) and (d). It is clear that the isothermal DSC curves of the studied MGs are similar, i.e., the incubation time prolongs and the whole crystallization time increases with the decrease of T_a, implying a slower crystallization process.

3.3. Thermodynamics and kinetics

In the theoretical framework of thermodynamics, c_p plays an essential role, and thus the accurate measurement of c_p is of great importance. Fig. 3(a) and (b) shows the temperature dependence of c_p measured by the temperature step method for the amorphous (half-filled diamonds), crystalline (filled circles) and liquid (unfilled triangles) states of $Gd_{55}Co_{17.5}Al_{27.5}$ and $Gd_{55}Co_{22.5}Al_{22.5}$ alloys, respectively. The function curves between temperature and the specific heat capacities
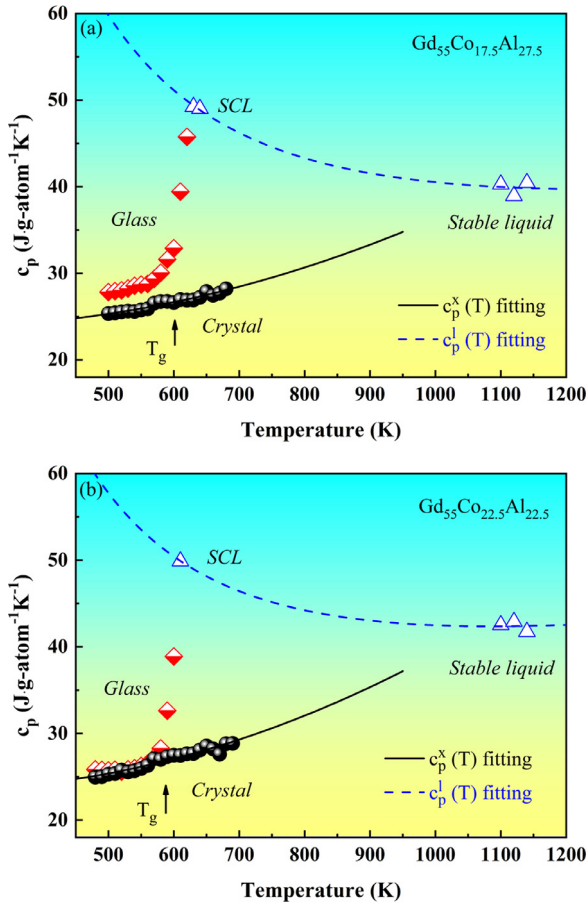
Fig. 3. All measured c_p data points for crystalline state (fill circles), supercooled liquid (SCL) and stable liquid (unfilled triangles), and glassy state (half-filled diamonds) of Gd$_{55}$Co$_{17.5}$Al$_{27.5}$ (a) and Gd$_{55}$Co$_{22.5}$Al$_{22.5}$ (b) alloys. The curves for liquid and crystalline state are fitted using Eqs. (2) and (3), respectively.

of the crystal (c_p^x(T)) and the liquid (c_p^l(T)) are fitted according to Kubaschewski et al. [43], with the following formulas:

$$c_p^l(T) = 3R + aT + bT^{-2} \tag{2}$$

$$c_p^x(T) = 3R + cT + dT^2 \tag{3}$$

where R is the universal gas constant, a, b, c and d are fitting constants as listed in Table 1. There is a common feature of these two alloys that a step in the specific heat capacity of glassy state (Δc_p) is observed near T_g, which is the difference between the extrapolated c_p value of supercooled liquid and the extrapolated c_p value of the glass at T_g [44]. The values of Δc_p for Gd$_{55}$Co$_{17.5}$Al$_{27.5}$ and Gd$_{55}$Co$_{22.5}$Al$_{22.5}$ BMGs are 11.35 and 13.20 J g-atom^{-1} K^{-1}, respectively, which are close to $3R/2$ (12.47 J g-atom^{-1} K^{-1}) and consistent with the reported results [44].

Combining the measured c_p data and the DSC scan data including T_m, enthalpy of fusion (ΔH_m) and entropy of fusion (ΔS_m), the functions of enthalpy difference $\Delta H^{l-x}(T)$ and entropy difference $\Delta S^{l-x}(T)$ for liquid and crystal are evaluated by the following equations:

$$\Delta H^{l-x}(T) = \Delta H_m - \int_T^{T_m} \Delta c_p^{l-x}(T')\, dT' \tag{4}$$

$$\Delta S^{l-x}(T) = \Delta S_m - \int_T^{T_m} \frac{\Delta c_p^{l-x}(T')}{T'}\, dT' \tag{5}$$

where $\Delta c_p^{l-x}(T)$ is the difference of c_p between liquid and crystal calculated by subtracting $c_p^x(T)$ from $c_p^l(T)$. Fig. 4 exhibits the $\Delta H^{l-x}(T)$ and $\Delta S^{l-x}(T)$ for Gd$_{55}$Co$_{17.5}$Al$_{27.5}$ and Gd$_{55}$Co$_{22.5}$Al$_{22.5}$ BMGs plotted as a function of temperature. Obviously, the $\Delta H^{l-x}(T)$ and $\Delta S^{l-x}(T)$ show the same trend, and both of them decrease with reducing temperature. The superheated liquid transforms to the supercooled liquid cooling through T_m, subsequently, the supercooled liquid freezes to a glass below T_g. Consequently, the residual enthalpy is frozen in the glassy state and can be released via enthalpy relaxation by annealing below T_g. The constant enthalpy and entropy difference between glassy and crystalline states results from the small difference of c_p between the glass and crystal as shown in Fig. 3. In addition, the Kauzmann temperatures (T_K) at which the entropies of liquid and crystal would coincide [45], are 541 and 535 K for Gd$_{55}$Co$_{17.5}$Al$_{27.5}$ and Gd$_{55}$Co$_{22.5}$Al$_{22.5}$ BMGs, respectively.

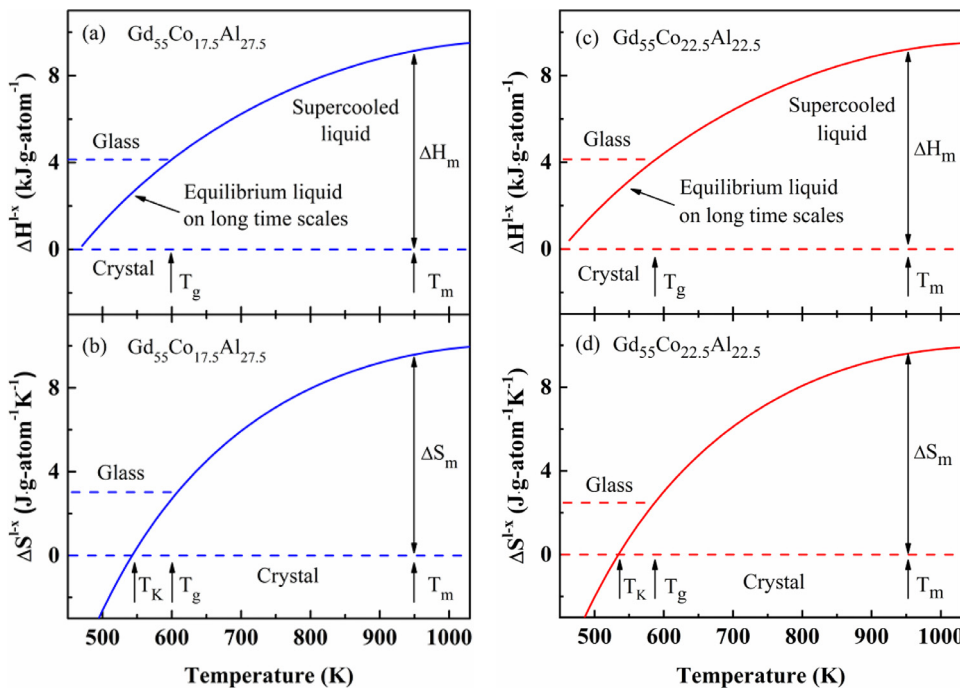**Fig. 4.** Calculated functions of enthalpy and entropy between liquid and crystalline state for Gd$_{55}$Co$_{17.5}$Al$_{27.5}$ (a) and Gd$_{55}$Co$_{22.5}$Al$_{22.5}$ (b) alloys. T_g, T_m, T_K, ΔH_m and ΔS_m are indicated.
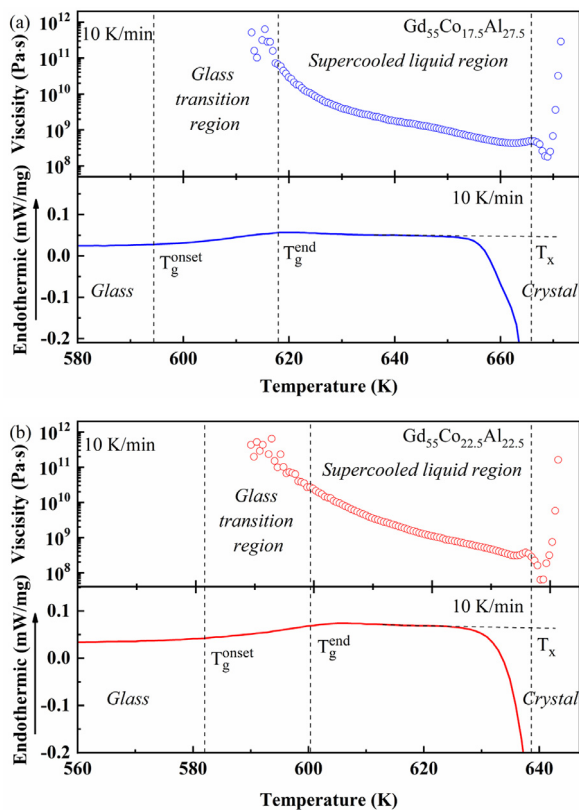
Fig. 5. Temperature dependence of viscosity at the vicinity of T_g for $Gd_{55}Co_{17.5}Al_{27.5}$ (a) and $Gd_{55}Co_{22.5}Al_{22.5}$ (b). Additionally, DSC traces of the glass formers measured with the same heating rate of 10 K/min are included, and the characteristic temperatures are confirmed by tangent method.

For further understanding GFA from the view of kinetics, the viscosity of $Gd_{55}Co_{17.5}Al_{27.5}$ and $Gd_{55}Co_{22.5}Al_{22.5}$ BMGs in the supercooled liquid region was measured and shown in Fig. 5(a) and (b), respectively. The DSC traces measured with the same heating rate are placed below the viscosity data. It is clear that these two alloys exhibit the same trend. With the temperature increasing from the onset temperature of glass transition (T_g^{onset}) to the end temperature of glass transition (T_g^{end}), the viscosity is discrete and drops gradually. Further increasing the temperature beyond T_g^{end}, the viscosity decreases drastically from the magnitude of 10^{11} to 10^7, reflecting the softening behavior of the BMGs in their supercooled liquid regions in which after full relaxation, the atoms begin to rearrange, forming numerous clusters with different central atoms [46]. As the temperature rises above T_x, the viscosity increases sharply and reaches the same order of magnitude as that of glassy state, signifying that this method is reliable in measuring viscosity, especially for supercooled liquid region. It is noteworthy that the supercooled liquid regions demarcated by the viscosity curve are consistent with those obtained from the DSC trace as marked in Fig. 5, and it is clear that $Gd_{55}Co_{17.5}Al_{27.5}$ presents a broader supercooled liquid region.

3.4. Thermal expansion behavior

Dilatometric measurements were performed to investigate the thermal expansion behavior of the studied BMGs. Fig. 6(a) presents the typical thermal expansion traces of $Gd_{55}Co_{17.5}Al_{27.5}$ and $Gd_{55}Co_{22.5}Al_{22.5}$ BMGs. The transition temperature (T_r) and T_g obtained from TMA are defined in the inset. The dilatation curve can be roughly divided into four regions. Below T_r, the temperature dependence of thermal expansion is nearly linear. In the temperature interval from T_r to T_g, the thermal expansion slows down and comes to stop at a certain temperature, which is similar with the phenomena reported in Fe-based [47], Zr-
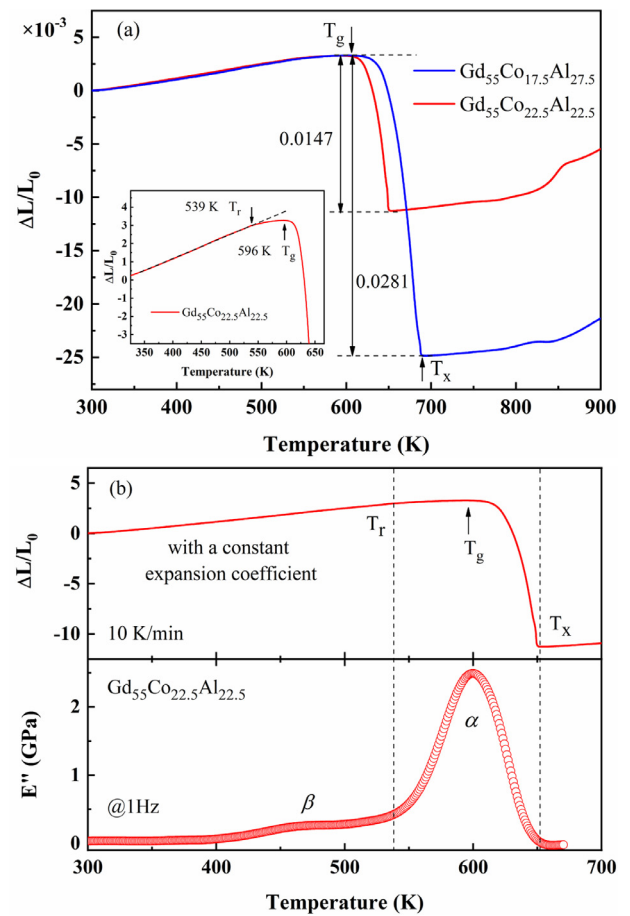

Fig. 6. (a) Linear thermal expansion curves with a heating rate of 10 K/min for $Gd_{55}Co_{17.5}Al_{27.5}$ and $Gd_{55}Co_{22.5}Al_{22.5}$ BMGs, the inset presents the definition of T_r and T_g. (b) Linear thermal expansion curves combined with temperature dependence of the loss modulus (E'') measured at 1 Hz with a heating rate of 2 K/min for the $Gd_{55}Co_{22.5}Al_{22.5}$ BMG.

based [48] and other Gd-based [49] MGs. Subsequently, the length of sample undergoes a remarkable decrease due to the softening behavior in supercooled liquid region and the applied force [50]. After complete crystallization, the length re-increases with increasing temperature. It is obvious that the thermal expansion behaviors of these two alloys in the supercooled liquid region are significantly different. For comparison, the values of contraction in supercooled liquid region are calculated as shown in Fig. 6(a), which are 0.0281 and 0.0147 for $Gd_{55}Co_{17.5}Al_{27.5}$ and $Gd_{55}Co_{22.5}Al_{22.5}$ BMGs, respectively.

3.5. Magnetocaloric effect

The temperature dependence of magnetization curves for $Gd_{55}Co_{17.5}Al_{27.5}$ and $Gd_{55}Co_{22.5}Al_{22.5}$ glassy rods are shown in Fig. 7(a). A sharp magnetic transition from FM to PM state is observed where the magnetization decreases dramatically upon heating for both alloys. The ordering temperatures (T_C) defined as the temperature corresponding to the maximum value of $|dM/dT|$ for $Gd_{55}Co_{17.5}Al_{27.5}$ and $Gd_{55}Co_{22.5}Al_{22.5}$ BMGs are 95 and 104 K, respectively, as marked in the inset of Fig. 7(a).

ΔS_M is used to evaluate the MCE of magnetic refrigerants. The corresponding ΔS_M caused by the applied magnetic field change can be calculated by integrating the Maxwell relation described as the following equation [51]:

$$\Delta S_M(T, H) = \int_{H_{min}}^{H_{max}} \left(\frac{\partial M}{\partial T} \right)_H dH \qquad (6)$$
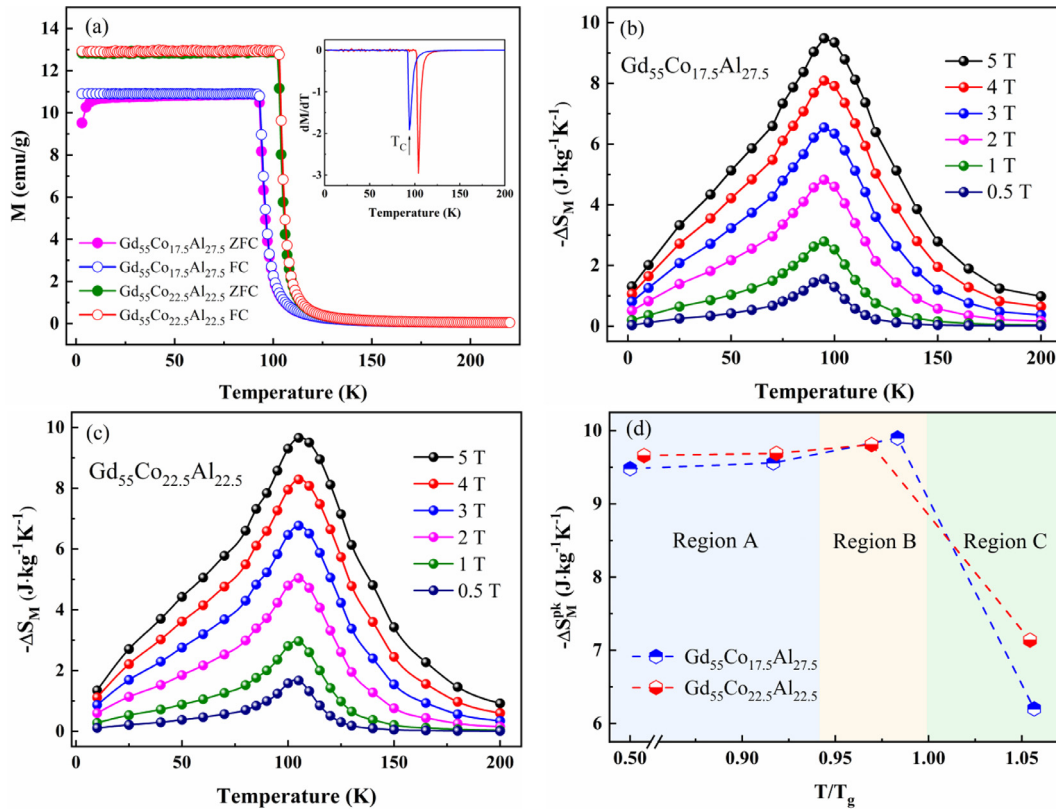
Fig. 7. (a) Temperature dependence of the M_{ZFC} and M_{FC} curves under an applied magnetic field of 100 Oe for $Gd_{55}Co_{17.5}Al_{27.5}$ and $Gd_{55}Co_{22.5}Al_{22.5}$ BMGs, $-\Delta S_M$ as a function of temperature under a magnetic field change of 0.5, 1, 2, 3, 4 and 5 T for $Gd_{55}Co_{17.5}Al_{27.5}$ (b) and $Gd_{55}Co_{22.5}Al_{22.5}$ (c) BMGs, and (d) the relationship between $-\Delta S_M^{pk}$ and T_a (the annealing time was set as 60 min for all temperatures), the temperature axis is normalized with T_g. For comparison, the as-cast samples are considered to be annealed at RT (300 K).

Table 2
Critical diameter (d_c) and magnetocaloric parameters of $Gd_{55}Co_{17.5}Al_{27.5}$, $Gd_{55}Co_{22.5}Al_{22.5}$ and other ternary Gd-based BMGs taken from Refs: magnetic transition temperature (T_C) obtained under a magnetic field of 100 Oe, peak value of the magnetic entropy change ($|\Delta S_M^{pk}|$) and relative cooling power (RCP) under a magnetic field of 5 T.

Composition	d_c (mm)	T_C (K)	$|\Delta S_M^{pk}|$ (J kg^{-1} K^{-1})	RCP (J kg^{-1})	Reference
$Gd_{55}Co_{17.5}Al_{27.5}$	8	95	9.48	843	This work
$Gd_{55}Co_{22.5}Al_{22.5}$	3	104	9.66	808	This work
$Gd_{60}Co_{25}Al_{15}$	5	124	9.3	800	[19]
$Gd_{55}Ni_{20}Al_{25}$	3.5	71	7.98	782	[18]
$Gd_{55}Fe_{25}Al_{20}$	–	230	3.77	811	[81]

where H_{min} and H_{max} represent the minimum and maximum values of applied magnetic field. In this study, $H_{min} = 0$ T and $H_{max} = 5$ T. Fig. 7(b) and (c) shows the field and temperature dependence of $-\Delta S_M$ for $Gd_{55}Co_{17.5}Al_{27.5}$ and $Gd_{55}Co_{22.5}Al_{22.5}$ BMGs. It is obvious that the $-\Delta S_M$ increases and the position of the peak magnetic entropy change ($|\Delta S_M^{pk}|$) shifts to higher temperature with the increase of magnetic field. The $|\Delta S_M^{pk}|$ of $Gd_{55}Co_{17.5}Al_{27.5}$ and $Gd_{55}Co_{22.5}Al_{22.5}$ under the field change of 5 T reach as high as 9.48 and 9.66 J kg^{-1} K^{-1} around T_C, which are comparable to those of most ternary Gd-based BMGs as listed in Table 2. Moreover, it is clear that the combination of the relatively large value of $|\Delta S_M^{pk}|$ and the broad ΔS_M hump at the vicinity of T_C enables a large working temperature range. To better understand the MCE, heat treatments are performed on base of the results of Section 3.2. The effect of T_a on $|\Delta S_M^{pk}|$ can be divided into three regions as displayed in Fig. 7(d), which will be discussed in the following section.

The relative cooling power (RCP) is another important parameter to evaluate the efficiency in a refrigeration cycle. In this study, the value of RCP was obtained by multiplying $|\Delta S_M^{pk}|$ and δT_{FWHM} [52,53]. The

values of RCP for $Gd_{55}Co_{17.5}Al_{27.5}$ and $Gd_{55}Co_{22.5}Al_{22.5}$ BMGs are 843 and 808 J kg^{-1}, which are remarkably larger than that of $Gd_5Si_2Ge_2$ [54] and $Gd_5Si_2Ge_{1.9}Fe_{0.1}$ [55] crystalline refrigerants as well as most Gd-based amorphous refrigerants as listed in Table 2. The high RCP can be attributed to the relatively large ΔS_M and the broad δT_{FWHM} extended by the glassy structure.

4. Discussion

4.1. Thermal stability of the glass formers

To further confirm the existence of T_{ct}, the studied enthalpy of the BMGs is defined as the integration of the heat flow from T_1 (~583 K for $Gd_{55}Co_{17.5}Al_{27.5}$, ~550 K for $Gd_{55}Co_{22.5}Al_{22.5}$) at which the structural relaxation starts to T_2 (638 K for $Gd_{55}Co_{17.5}Al_{27.5}$, 620 K for $Gd_{55}Co_{22.5}Al_{22.5}$) where all the samples are in the supercooled liquid region, indicating the enthalpy is assumed to be the same regardless of the thermal history [56]. As shown in Fig. 8(a), the enthalpy first
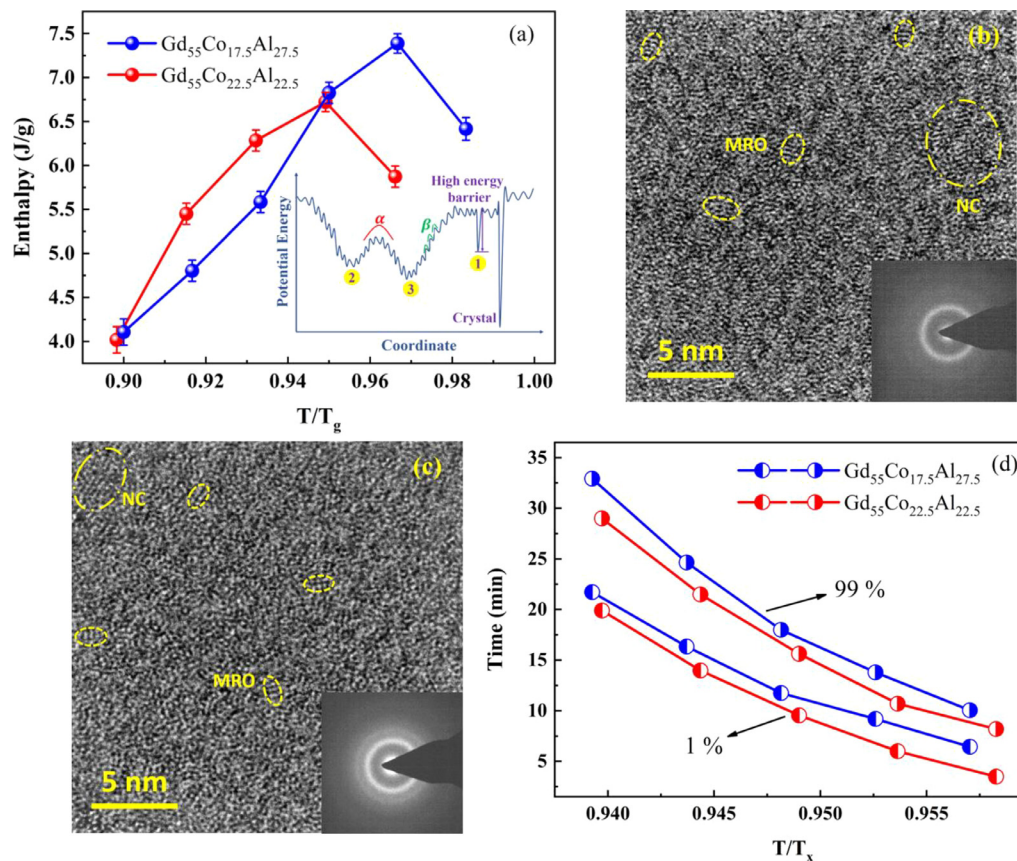
Fig. 8. (a) Enthalpy versus T_g scaled T_a, and the inset exhibits the schematic diagram of PEL. HRTEM and SAED images of the $Gd_{55}Co_{17.5}Al_{27.5}$ (b) and $Gd_{55}Co_{22.5}Al_{22.5}$ (c) BMGs annealed at T_{ct} for 60 min, and (d) temperature dependence of crystallization time of 1% and 99% for $Gd_{55}Co_{17.5}Al_{27.5}$ and $Gd_{55}Co_{22.5}Al_{22.5}$ BMGs.

increases with increasing T_a, indicating the enhancement of thermodynamic stability. During the isothermal process, the nonequilibrium glass relaxes towards the equilibrium supercooled liquid state which is a more thermodynamically stable state. Consequently, the relaxed samples need to absorb more energy to active crystallization. When the T_a is above T_{ct}, the enthalpy decreases. The $Gd_{55}Co_{17.5}Al_{27.5}$ BMG shows higher thermal stability with respect to its higher T_{ct}, leading to a larger GFA. Fig. 8(b) and (c) displays the HRTEM images of these two BMGs annealed at their T_{ct}. The selected area electron diffraction (SAED) patterns in the inset show diffuse halo rings without any diffracted spots, verifying their amorphous structure. However, a few MRO or even scarce NC structures embedded in the disordered matrix can be observed. When T_a is beyond T_{ct}, a certain number of clusters will arise and the release of free volume becomes more significant, which leads to the reduction of enthalpy. By annealing below T_g, MGs regains its mobility and relax towards supercooled liquid state corresponding to the states with lower potential energy in potential energy landscape (PEL) [36,39]. As shown in the inset of Fig. 8(a), there are many possible metastable states in amorphous alloys. The amorphous alloy is more stable in thermodynamics at lower energy states (state 2) and with higher energy barrier corresponds to higher kinetic stability (state 1) [57]. T_g just reflects the dynamic stability, i.e., the energy barrier of states in PEL. Therefore, there may be some local drop with the increase of T_a as shown in Fig. 2(a) and (b).

Sluggish crystallization is another reflection of the thermal stability of glass-forming alloys. Fig. 8(d) exhibits temperature dependence of crystallization time at different crystallization fraction of 1% and 99% which can be obtained by integrating the crystallization peak to a certain time on the measured isothermal DSC curves. Apparently, the crystallization time of $Gd_{55}Co_{17.5}Al_{27.5}$ is longer than that of $Gd_{55}Co_{22.5}Al_{22.5}$ at every reduced temperature, even though the

isothermal annealing temperatures of $Gd_{55}Co_{17.5}Al_{27.5}$ are higher than those of $Gd_{55}Co_{22.5}Al_{22.5}$ as shown in Fig. 2(c) and (d). This result is consistent with the larger supercooled liquid region for $Gd_{55}Co_{17.5}Al_{27.5}$. It is worth noting that the difference of crystallization time for 1% between $Gd_{55}Co_{17.5}Al_{27.5}$ and $Gd_{55}Co_{22.5}Al_{22.5}$ increases with the increase of temperature, indicating the $Gd_{55}Co_{17.5}Al_{27.5}$ BMG possesses higher crystallization resistance even at high T/T_x over 0.955. The crystallization process of amorphous alloys is extremely sensitive to temperature. The relatively large crystallization resistance at high temperature which may resulting from the competition of two large clustered structural units [37,58] is a guarantee of high thermal stability of MGs. To further confirm the relatively sluggish crystallization, the Kissinger's method was performed by a serious of DSC curves with different heating rates [59]. The values of the effective activation energy for glass transition (E_g) and crystallization (E_x) were then determined to be 8.07 and 5.11 eV for $Gd_{55}Co_{17.5}Al_{27.5}$ while 7.75 and 4.89 eV for $Gd_{55}Co_{22.5}Al_{22.5}$. The larger values of E_g and E_x for the $Gd_{55}Co_{17.5}Al_{27.5}$ BMG lead to higher energy barrier for the transition from glassy state to crystalline state, which corresponds to a more stable supercooled liquid region [60]. As a result, the sluggish crystallization kinetics of the $Gd_{55}Co_{17.5}Al_{27.5}$ BMG contributes to the high thermal stability, and therefore results in a better GFA.

4.2. Thermodynamic and kinetic analyses

At present, it is of great difficulty to directly observe the microstructure of MGs, and thus the explanation of GFA from thermodynamic and kinetic aspects is more available [61]. From the thermodynamic aspect, the Gibbs free energy difference between liquids and crystal (ΔG^{l-x}) is considered to correlate with GFA, that is, smaller ΔG^{l-x} means a lower driving force for crystallization, inclining to form amorphous
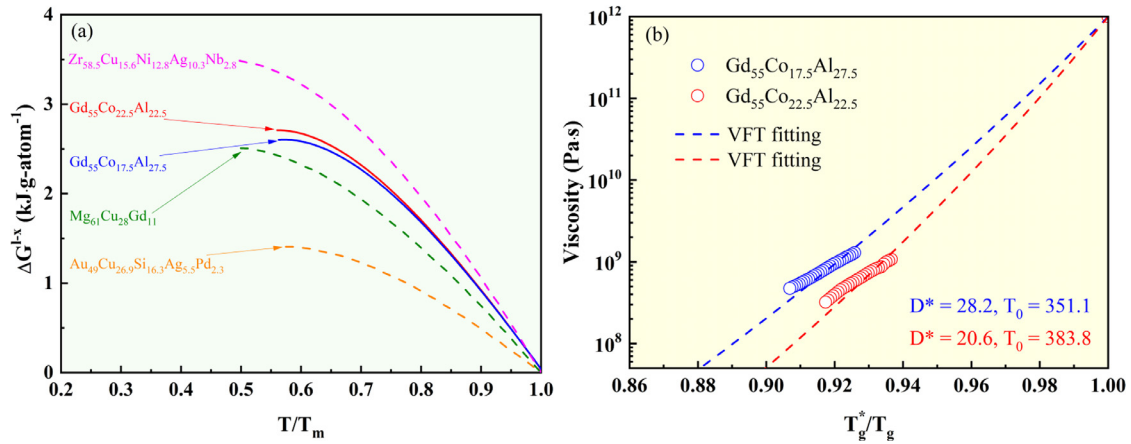
Fig. 9. (a) Gibbs free energy functions of the studied Gd-based alloys investigated in this study (solid lines), together with other four typical metallic glass formers (dashed lines). The temperature axis is normalized with T_m. (b) Viscosity versus T_g^*/T for $Gd_{55}Co_{17.5}Al_{27.5}$ and $Gd_{55}Co_{22.5}Al_{22.5}$ BMGs, and the plots are fitted by VFT equation.

alloys [62,63]. $\Delta G^{l-x}(T)$ is calculated from Eq. (7).

$$\Delta G^{l-x}(T) = \Delta H^{l-x}(T) - T\Delta S^{l-x}(T) \tag{7}$$

Fig. 9(a) shows the calculated $\Delta G^{l-x}(T)$ curves of $Gd_{55}Co_{17.5}Al_{27.5}$ and $Gd_{55}Co_{22.5}Al_{22.5}$ together with the curves of Fe-, Zr-, Mg- and Au-based metallic glass formers taken from literatures [33,34,36,64]. The temperature axis is normalized by T_m to allow an overall comparison. According to the thermodynamic theory, the driving force for crystallization can be characterized by ΔG^{l-x} approximately [61]. As shown in Fig. 9(a), $Gd_{55}Co_{17.5}Al_{27.5}$ and $Gd_{55}Co_{22.5}Al_{22.5}$ BMGs show the expected behavior, namely, the ΔG^{l-x} is negatively correlated with GFA. Larger ΔG^{l-x} for the $Gd_{55}Co_{22.5}Al_{22.5}$ BMG means that the crystallization of this alloy dominates the competition with glass transition during cooling from liquid. However, simply thermodynamic considerations such as ΔG^{l-x} is insufficient to accurately predicate the GFA, especially for different alloy systems. The true thermodynamic driving force for nucleation is determined by the chemical potential difference between two states [65]. Nevertheless, ΔG^{l-x} can still be used to evaluate the GFA preliminarily for the same alloy system.

In terms of dynamics, viscosity and fragility concepts proposed by Angell are the widely accepted approaches to elucidate the possible mechanisms for GFA [66]. Liquids are stronger when the thermophysical properties such as viscosity, diffusivity, relaxation time, etc. show a more Arrhenius behavior [67]. Generally, the large viscosity of supercooled liquid corresponds to sluggish kinetics, and enhances the thermal stability of supercooled liquid region. As shown in Fig. 9(b), $Gd_{55}Co_{17.5}Al_{27.5}$ exhibits a larger viscosity in its supercooled liquid region than $Gd_{55}Co_{22.5}Al_{22.5}$, and the difference increases with increasing of temperature, indicating that the $Gd_{55}Co_{17.5}Al_{27.5}$ alloy possesses more sluggish kinetics in the supercooled liquid region upon heating. The viscosity of MGs deviates from Arrhenius relation and can be fitted by the following Vogel–Fulcher–Tamman (VFT) equation:

$$\eta = \eta_0 \exp\left(\frac{D^* \cdot T_0}{T - T_0}\right) \tag{8}$$

here, η_0 is the pre-exponential factor, D^* is the fragility parameter, and T_0 is VFT temperature, which is far below the experimentally measured T_g. The best fitting results are listed in Table 1. Obviously, the $Gd_{55}Co_{17.5}Al_{27.5}$ BMG shows a stronger behavior in consideration of its larger values of D^* and T_g/T_0 (1.72, which is 1.47 for $Gd_{55}Co_{22.5}Al_{22.5}$). Furthermore, the fragility index m corresponding to the slope of viscosity $(m = d(\log\eta)/d(\frac{T_g^*}{T}))$ is another common parameter to characterize the fragility of a glass former. According to Ref. [68], m can be derived from D^* $(m = 16 + \frac{590}{D^*})$. The m value of amorphous alloys is usually between 25 and 100. Generally, amorphous alloys with m less than 35 are

classified as strong glass formers including Zr-, Cu-, Mg-based MGs [57]. The m values for $Gd_{55}Co_{17.5}Al_{27.5}$ and $Gd_{55}Co_{22.5}Al_{22.5}$ BMGs are 36.9 and 44.6, respectively, indicating that $Gd_{55}Co_{17.5}Al_{27.5}$ is a stronger glass former. Indeed, m reflects the activation energy of liquid flow. A collective rearrangement of groups of particles is predominant in fragile liquids, compared with small local rearrangements in strong liquids [46]. Thus, the $Gd_{55}Co_{17.5}Al_{27.5}$ BMG possess more sluggish crystallization kinetics and tend to be a better glass former.

Relaxation is another characteristic of glass, which is of great significance to understand the intrinsic dynamic characteristics of glass-forming alloys. Fig. 10(a) and (b) displays the temperature dependent loss modulus E'' of $Gd_{55}Co_{17.5}Al_{27.5}$ and $Gd_{55}Co_{22.5}Al_{22.5}$ BMGs exhibiting two distinct peaks, i.e., a sharp α-relaxation peak at the vicinity of T_g and a pronounced β-relaxation peak around 0.75 T_g. It is clear that the peak temperature of the α-relaxation shifts to higher temperature with the frequency increasing from 0.2 to 2 Hz. As the α-relaxation is closely related to glass transition and behaves in Arrhenius type [69], the activation energy of α-relaxation (E_α) can be derived from Arrhenius plots as shown in the insets of Fig. 10(a) and (b). According to Ref. [70], the fragility index m can be determined from E_α ($m = \frac{E_\alpha}{RT_g \ln 10}$, in this study, T_g is the peak temperature of the α-relaxation under 1 Hz). The values of m are 36.7 ± 1.9 and 44.2 ± 2 for $Gd_{55}Co_{17.5}Al_{27.5}$ and $Gd_{55}Co_{22.5}Al_{22.5}$ BMGs, respectively, which are highly consistent with the values obtained from the analysis of viscosity. Fig. 10(c) and (d) exhibits the frequency dependence of β-relaxation and the insets are the Arrhenius plots of $Gd_{55}Co_{17.5}Al_{27.5}$ and $Gd_{55}Co_{22.5}Al_{22.5}$ BMGs. Due to the lack of distinct peak corresponding to β-relaxation, the method presented in Ref. [71] was performed to obtain the activation energy of β-relaxation (E_β). The values of E_β for $Gd_{55}Co_{17.5}Al_{27.5}$ and $Gd_{55}Co_{22.5}Al_{22.5}$ BMGs are 24.8 and 23.8 RT_g, respectively. Actually, the value of E_β for different MGs is in the range of 20 - 30 RT_g, implying the coherent nature of β-relaxation despite of the various forms of β-relaxation for different amorphous alloys. Nevertheless, there are some difference on the style of β-relaxation for these two glass formers. As shown in Fig. 10(c) and (d), the β-relaxation of the $Gd_{55}Co_{17.5}Al_{27.5}$ BMG displays as a broader hump compared with that of the $Gd_{55}Co_{22.5}Al_{22.5}$ BMG, resulting from the open network structures with strong directional bonds which resist temperature-induced structural change in strong glass former [72]. The results of DMA also demonstrate that the $Gd_{55}Co_{17.5}Al_{27.5}$ BMG shows a stronger behavior.

The above analyses indicate that the better GFA of $Gd_{55}Co_{17.5}Al_{27.5}$ alloy can be attributed to its stronger liquid behavior and lower driving force for crystallization. In order to understand the structural origin of the different GFA of these two glass formers, the densities of MGs were measured at RT using Archimedean technique, and the relative density
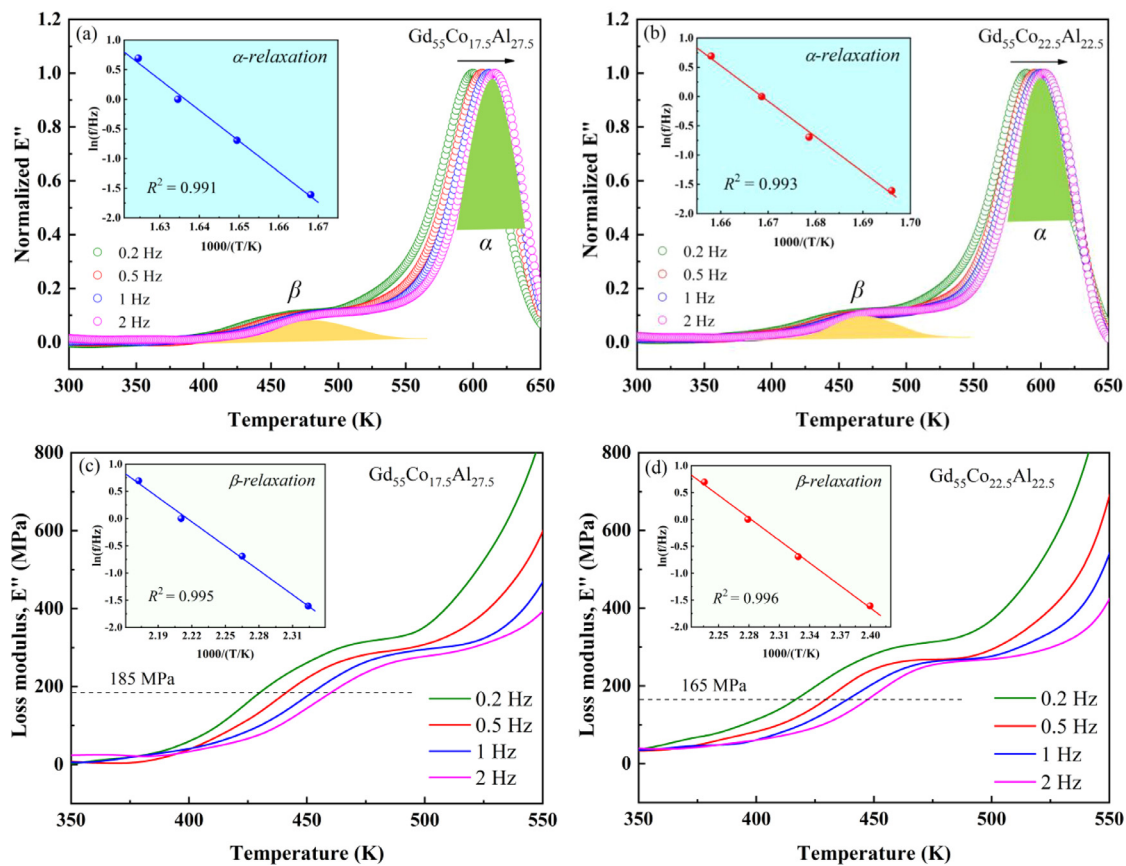
Fig. 10. Temperature dependence of loss modulus (E'') for $Gd_{55}Co_{17.5}Al_{27.5}$ (a), (c) and $Gd_{55}Co_{22.5}Al_{22.5}$ (b), (d) BMGs at a heating rate of 2 K/min from 0.2 to 2 Hz. The green region identifies α-relaxation and the yellow region represents β-relaxation. The insets show the Arrhenius plots. (For interpretation of the references to colour in this figure legend, the reader is referred to the web version of this article).

change was carried out ($\Delta\rho = [\rho_c - \rho_0]/\rho_0$, where ρ_c is the density of crystal, and ρ_0 is the density of glass). According to previous study, the density of the amorphous state is closely related to glass formation and the relative density change can reflect the fragility and concentration of flow units [73,74]. In this study, the values of $\Delta\rho$ are 0.44% and 1.21% for $Gd_{55}Co_{17.5}Al_{27.5}$ and $Gd_{55}Co_{22.5}Al_{22.5}$ BMGs, respectively, which manifests that the concentration of flow units for the $Gd_{55}Co_{17.5}Al_{27.5}$ BMG is lower than that of the $Gd_{55}Co_{22.5}Al_{22.5}$ BMG. For MGs with lower concentration of flow units, the corresponding metallic liquid has larger viscosity and smaller fragility, leading to a higher resistance for the rearrangement of atoms from liquid to crystal. After complete crystallization, the flow units will disappear, resulting in the reduction of volume and the augmentation of density. On the other hand, flow units can be regarded as nucleation points due to the relatively high structural fluctuation and energy fluctuation. Therefore, the relatively lower driving force for crystallization of the $Gd_{55}Co_{17.5}Al_{27.5}$ BMG may originate from the lower concentration of flow units comparing with the $Gd_{55}Co_{22.5}Al_{22.5}$ BMG. Based on the above discussion, thermodynamic and kinetic characteristics may be connected by flow units to evaluate GFA.

4.3. Correlation between GFA and thermal expansion

MGs may present some unique thermal expansion phenomena, and the study of thermal expansion behavior is conducive to understand GFA. As shown in Fig. 6(b), a correlation between thermal expansion and dynamical relaxation can be established. The T_r confirmed by thermal expansion corresponds to the transition region from β-relaxation to α-relaxation. In other words, below T_r, although β-relaxation has been progressing in a wide temperature range, no obvious change in ther-

mal expansion behavior can be detected. Once α-relaxation is activated, the thermal expansion deviates from the linear behavior, indicating that the drastic contraction is controlled by α-relaxation. At temperatures well below T_g, the configurational contribution to thermal expansion is structurally frozen, and the vibration dominates the thermal expansion process. With temperatures passing through T_g, the configurational contribution to thermal expansion becomes significant and more prominent with the increase of temperature, which can counteract the positive vibrational contribution and lead to the shrinkage [48]. Compared with the $Gd_{55}Co_{22.5}Al_{22.5}$ BMG, the $Gd_{55}Co_{17.5}Al_{27.5}$ BMG possesses broader supercooled liquid regions and higher relaxation temperatures, and thus, the contraction resulting from the configurational contribution is more remarkable as shown in Fig. 6(a). Based on the above analyses, the value of contraction in supercooled liquid region may be used to evaluate GFA within the same alloy system. However, a more precise relationship between the value of contraction and GFA depends on further research.

4.4. Magnetic transition

The inset of Fig. 11(a) displays the isothermal magnetization (M–H) curves of the as-cast $Gd_{55}Co_{17.5}Al_{27.5}$ BMG measured at a serious of temperatures with the external magnetic fields varying from 0 to 5 T. At low temperatures, the magnetization increases sharply by applying a quite small field, and then reaches a saturation with the further increase of magnetic field, which shows a typical FM behavior. As the temperature increases from 2 to 200 K, the saturation magnetization decreases gradually from near 200 to less than 25 emu/g, undergoing a magnetic transition from FM to PM. Fig. 11(a) exhibits the corresponding Arrott plots of $Gd_{55}Co_{17.5}Al_{27.5}$ glassy rod derived from the M–H curves.

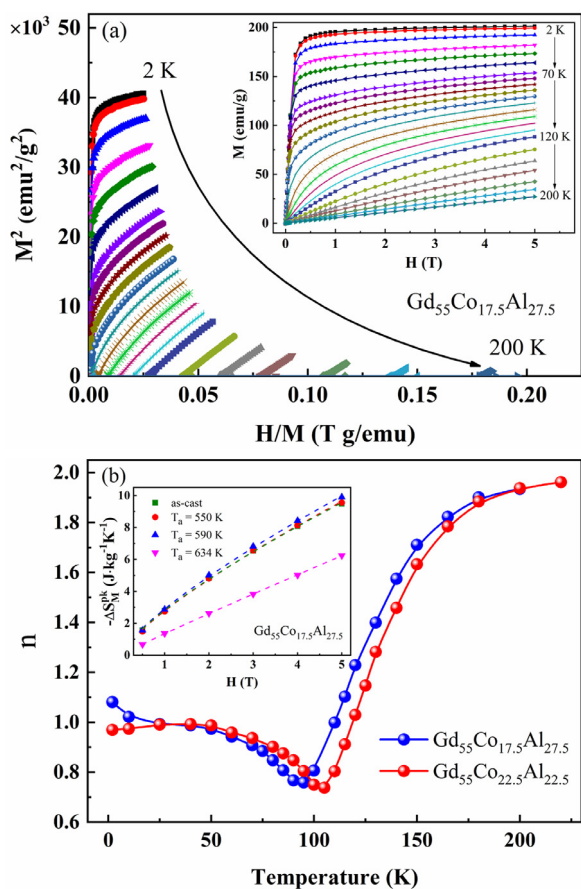**Fig. 11.** (a) Arrott plots and isothermal magnetization curves for the as-cast $Gd_{55}Co_{17.5}Al_{27.5}$ BMG, and (b) temperature dependence of the exponent characterizing the field dependence of ΔS_M for $Gd_{55}Co_{17.5}Al_{27.5}$ and $Gd_{55}Co_{22.5}Al_{22.5}$ BMGs. The inset of (b) exhibits the $-\Delta S_M^{pk}$ as a function of H around T_C for the $Gd_{55}Co_{17.5}Al_{27.5}$ BMGs annealed at different temperatures, and the dash lines represent the fitting curves according to $\Delta S_M^{pk} = H^n$.

According to the Banerjee's theory, the positive slopes is considered as the characteristic of a second-order magnetic transition; otherwise, it is identified as a first-order magnetic transition [75]. It is evident that no negative slopes can be observed on Arrott plots within the whole temperature range, providing a proof of a second-order FM to PM transition in the $Gd_{55}Co_{17.5}Al_{27.5}$ BMG, implying this magnetic refrigerant possesses low hysteresis.

A deeper understanding of the second-order magnetic transition observed in $Gd_{55}Co_{17.5}Al_{27.5}$ and $Gd_{55}Co_{22.5}Al_{22.5}$ BMGs can be obtained based on the theory proposed by Franco et al. [76]. The calculated n versus temperature is shown in Fig. 11(b), which can be divided into three temperature regions [77]. When the temperatures are well above T_C, the material exhibits paramagnetic behavior, and the value of n tends to 2 according to the Curie-Weiss law. With the temperatures well below T_C, magnetization is temperature independent and the value of n is towards 1 as the consequence of Eq. (6). The values of n are 0.759 and 0.738 for $Gd_{55}Co_{17.5}Al_{27.5}$ and $Gd_{55}Co_{22.5}Al_{22.5}$ at T_C, respectively, which are consistent with the value predicted by the Arrott–Noakes equation [78], and confirm the nature of a fully amorphous structure. The temperature dependence of n further ascertains the second-order magnetic transition in the studied BMGs, which is a guarantee of low hysteresis losses and broader δT_{FWHM}.

The heterogeneity and complexity of BMGs are supposed to have an effect on MCE [20,79]. The Gd-based BMGs analyzed in this study exhibit excellent MCE, and ΔS_M can be further enhanced by structural adjustment through annealing as shown in Fig. 7(d). If T_a is much less than T_g (region A), annealing leads to structural relaxation and stress relief,

but the enhancement of $|\Delta S_M^{pk}|$ is insignificant due to the preservation of mainly short-range order (SRO) and a small number of MRO. In region B, $|\Delta S_M^{pk}|$ reaches its maximum (for the $Gd_{55}Co_{17.5}Al_{27.5}$ BMG, from 9.48 to 9.9 $J\,kg^{-1}\,K^{-1}$) resulting from the more complicated microstructure with a large number of SRO, increased MRO and even scarce NC structures as shown in Fig. 8(c), where amorphous phase is magnetically coupled [80]. However, as T_a is above T_g, $|\Delta S_M^{pk}|$ decreases sharply with the increase of T_a attributed to the formation of long-range ordered crystalline structures, which lead to the deterioration of saturation magnetization. Furthermore, annealing treatment can change the relationship between ΔS_M and magnetic field. The inset of Fig. 11(b) displays the magnetic field dependence of $-\Delta S_M^{pk}$ for the $Gd_{55}Co_{17.5}Al_{27.5}$ BMG. It is clear that the samples annealed in region A and region B (the values of n are 0.768 and 0.773, respectively) except for region C ($n = 0.951$) exhibit similar tendency to the as-cast BMG ($n = 0.759$). This difference could be understood considering the fact that n value depends on the degree of magnetic frustration and structural heterogeneity [24]. The magnetic frustration decreases with increasing crystalline degree due to the easy magnetization direction of crystal. Smaller magnetic frustration leads to softer tendency for the magnetic moment to align with the external filed, and thus a larger n value is obtained in region C. Although the value of n for region C is the largest, the magnetic field of 46.2 T needs to be applied in order to reach the same magnitude of $|\Delta S_M^{pk}|$ for that of the as-cast sample, which is impossible under the existing experimental conditions. The large $|\Delta S_M^{pk}|$ and the relatively high value of n guarantee the excellent MCE of the samples in region A and region B.

5. Conclusions

In present work, novel ternary $Gd_{55}Co_{17.5}Al_{27.5}$ and $Gd_{55}Co_{22.5}Al_{22.5}$ BMGs with different critical size were synthesized. The critical diameter of $Gd_{55}Co_{17.5}Al_{27.5}$ BMG is up to 8 mm which is the largest in the ternary Gd-based BMGs reported up to now, while the GFA of the $Gd_{55}Co_{22.5}Al_{22.5}$ BMG is only 3 mm in critical diameter. The distinct difference on GFA was intensively illustrated from thermodynamic and kinetic aspects. Compared with the $Gd_{55}Co_{22.5}Al_{22.5}$ BMG, the $Gd_{55}Co_{17.5}Al_{27.5}$ BMG exhibits higher thermal stability manifested as a larger value of T_{ct} and more sluggish crystallization kinetics. The lower driving force for crystallization, stronger liquid behavior and higher concentration of flow units are considered to be the origination of larger GFA for the $Gd_{55}Co_{17.5}Al_{27.5}$ BMG. The investigation of linear thermal expansion exhibits that the $Gd_{55}Co_{17.5}Al_{27.5}$ BMG displays a larger contraction in supercooled liquid region, which may be used to evaluate GFA.

In addition, the MCE of $Gd_{55}Co_{17.5}Al_{27.5}$ and $Gd_{55}Co_{22.5}Al_{22.5}$ BMGs were studied. The effect of annealing on ΔS_M^{pk} can be divided into three regions depending on the microstructures induced by annealing. A more complicated microstructures encompassing mainly SRO, MRO and scarce NC structure can enhance ΔS_M. The combination of relatively large ΔS_M, predominant *RCP* as well as nearly negligible magnetic hysteresis guarantee the studied Gd-based BMGs promising magnetic refrigerants.

Declaration of competing interest

We have no known competing financial interests or personal relationships that could have appeared to influence the work reported in this paper.

References

[1] Q. Luo, W.H. Wang, Rare earth based bulk metallic glasses, J. Non-Cryst. Solids 355 (2009) 759–775.

[2] W.H. Wang, Bulk metallic glasses with functional physical properties, Adv. Mater. 21 (2009) 4524–4544.

[3] Q.S. Zeng, H.W. Sheng, Y. Ding, J.Z. Jiang, W.L. Mao, H.K. Mao, Long-range topological order in metallic glass, Science 332 (2011) 1404–1406.

[4] H.B. Yu, W.H. Wang, K. Samwer, The beta relaxation in metallic glasses: an overview, Mater. Today 16 (2013) 183–191.

[5] Q. Wang, J.J. Liu, Y.F. Ye, T.T. Liu, S. Wang, C.T. Liu, J. Lu, Y. Yang, Universal secondary relaxation and unusual brittle-to-ductile transition in metallic glasses, Mater. Today 20 (2017) 293–300.

[6] K.A. Gschneidner, V.K. Pecharsky, Magnetocaloric materials, Annu. Rev. Mater. Sci. 30 (2000) 387–429.

[7] N.R. Ram, M. Prakash, U. Naresh, N.S. Kumar, T.S. Sarmash, T. Subbarao, K.C.B. Naidu, Review on magnetocaloric effect and materials, J. Supercond. Nov. Magn. 31 (2018) 1971–1979.

[8] V. Franco, J.S. Blazquez, J.J. Ipus, J.Y. Law, A. Conde, Magnetocaloric effect: from materials research to refrigeration devices, Prog. Mater Sci. 93 (2018) 112–232.

[9] L. Manosa, A. Planes, Materials with giant mechanocaloric Effects: cooling by strength, Adv. Mater. 29 (2017) 1603607.

[10] J. Lyubina, Magnetocaloric materials for energy efficient cooling, J. Phys. D: Appl. Phys. 50 (2017) 053002.

[11] R. Barman, D. Kaur, Improved magnetocaloric effect in magnetron sputtered Ni–Mn–Sb–Al ferromagnetic shape memory alloy thin films, Vacuum 120 (2015) 22–26.

[12] O. Tegus, E. Bruck, K.H.J. Buschow, Transition-metal-based magnetic refrigerants for room-temperature applications, Nature 415 (2002) 150–152.

[13] M. Balli, S. Jandl, P. Fournier, Advanced materials for magnetic cooling: fundamentals and practical aspects, Appl. Phys. Rev. 4 (2017) 021305.

[14] Q. Luo, W.H. Wang, Magnetocaloric effect in rare earth-based bulk metallic glasses, J. Alloys Compd. 495 (2010) 209–216.

[15] Q. Luo, D.Q. Zhao, M.X. Pan, W.H. Wang, Magnetocaloric effect in Gd-based bulk metallic glasses, Appl. Phys. Lett. 89 (2006) 081914.

[16] J. Du, Q. Zheng, Y.B. Li, Q. Zhang, D. Li, Z.D. Zhang, Large magnetocaloric effect and enhanced magnetic refrigeration in ternary Gd-based bulk metallic glasses, J. Appl. Phys. 103 (2008) 023918.

[17] F.X. Qin, N.S. Bingham, H. Wang, H.X. Peng, J.F. Sun, V. Franco, S.C. Yu, H. Srikanth, M.H. Phan, Mechanical and magnetocaloric properties of Gd-based amorphous microwires fabricated by melt-extraction, Acta Mater 61 (2013) 1284–1293.

[18] F. Yuan, J. Du, B.L. Shen, Controllable spin-glass behavior and large magnetocaloric effect in Gd–Ni–Al bulk metallic glasses, Appl. Phys. Lett. 101 (2012) 032405.

[19] H. Fu, M. Zou, Magnetic and magnetocaloric properties of ternary Gd–Co–Al bulk metallic glasses, J. Alloys Compd. 509 (2011) 4613–4616.

[20] L. Xia, Q. Guan, D. Ding, M.B. Tang, Y.D. Dong, Magneto-caloric response of the $Gd_{60}Co_{25}Al_{15}$ metallic glasses, Appl. Phys. Lett. 105 (2014) 192402.

[21] Q.Y. Dong, B.G. Shen, J. Chen, J. Shen, J.F. Wang, H.W. Zhang, J.R. Sun, Large magnetic refrigerant capacity in $Gd_{71}Fe_3Al_{26}$ and $Gd_{65}Fe_{20}Al_{15}$ amorphous alloys, J. Appl. Phys. 105 (2009) 053908.

[22] H. Fu, Z. Ma, X.J. Zhang, D.H. Wang, B.H. Teng, E.A. Balfour, Table-like magnetocaloric effect in the Gd–Co–Al alloys with multi-phase structure, Appl. Phys. Lett. 104 (2014) 072401.

[23] Q. Zheng, L. Zhang, J. Du, Table-like magnetocaloric effect in Gd–Ni–Al amorphous/nanocrystalline composites, J. Phys. D Appl. Phys. 50 (2017) 355601.

[24] Q. Luo, N.D. Phuong, X.H. Kou, J. Shen, Controllable ferromagnetic/re-entrant spin glass state and magnetocaloric response of Gd–Er–Al–Co metallic glasses, J. Alloys Compd. 725 (2017) 835–839.

[25] L. Xue, L.L. Shao, Q. Luo, B.L. Shen, GdRECoAl (RE = Tb, dy and Ho) high-entropy glassy alloys with distinct spin-glass behavior and good magnetocaloric effect, J. Alloys Compd. 790 (2019) 633–639.

[26] Y.K. Fang, H.C. Chen, C.C. Hsieh, H.W. Chang, X.G. Zhao, W.C. Chang, W. Li, Structures and magnetocaloric effects of $Gd_{65-x}RE_xFe_{20}Al_{15}$ (x=0-20; RE=Tb, Dy, Ho, and Er) ribbons, J. Phys. D Appl. Phys. 109 (2011) 355601.

[27] Z.Y. Xu, X. Hui, E.R. Wang, J. Chang, G.L. Chen, Gd-Dy-Al-Co bulk metallic glasses with large magnetic entropy change and refrigeration capacity, J. Alloys Compd. 504 (2010) S146–S149 2010.

[28] J.L. Zhang, Z.G. Zheng, W.H. Cao, C.H. Shek, Magnetic behavior of Gd_4Co_3 metallic glass, J. Magn. Magn. Mater. 326 (2013) 157–161.

[29] Z. Li, D. Ding, L. Xia, Excellent magneto-caloric effect of a binary $Gd_{63}Ni_{37}$ amorphous alloy, Intermetallics 86 (2017) 11–14.

[30] L. Xue, J. Li, W.M. Yang, C.C. Yuan, B.L. Shen, Effect of Fe substitution on magnetocaloric effects and glass-forming ability in Gd-based metallic glasses, Intermetallics 93 (2018) 67–71.

[31] J.T. Huo, L.S. Huo, A. Inoue, J.Q. Wang, C.T. Chang, The magnetocaloric effect of Gd-Tb-Dy-Al-M (M = Fe, Co and Ni) high-entropy bulk metallic glasses, Intermetallics 58 (2015) 31–35.

[32] J. Li, L. Xue, W.M. Yang, C.C. Yuan, J.T. Huo, B.L. Shen, Distinct spin glass behavior and excellent magnetocaloric effect in $Er_{20}Dy_{20}Co_{20}Al_{20}RE_{20}$ (RE = Gd, Tb and Tm) high-entropy metallic glasses, Intermetallics 96 (2018) 90–93.

[33] B. Bochtler, O. Gross, I. Gallino, R. Busch, Thermo-physical characterization of the $Fe_{67}Mo_6Ni_{3.5}Cr_{3.5}P_{12}C_{5.5}B_{2.5}$ bulk metallic glass forming alloy, Acta Mater. 118 (2016) 129–139.

[34] M. Frey, R. Busch, W. Possart, I. Gallino, On the thermodynamics, kinetics, and sub-T_g relaxations of Mg-based bulk metallic glasses, Acta Mater. 155 (2018) 117–127.

[35] Z. Evenson, R. Busch, Equilibrium viscosity, enthalpy recovery and free volume relaxation in a $Zr_{44}Ti_{11}Ni_{10}Cu_{10}Be_{25}$ bulk metallic glass, Acta Mater. 59 (2011) 4404–4415.

[36] I. Gallino, M.B. Shah, R. Busch, Enthalpy relaxation and its relation to the thermodynamics and crystallization of the $Zr_{58.5}Cu_{15.6}Ni_{12.8}Al_{10.3}Nb_{2.8}$ bulk metallic glass–forming alloy, Acta Mater. 55 (2007) 1367–1376.

[37] O. Gross, B. Bochtler, M. Stolpe, S. Hechler, W. Hembree, R. Busch, I. Gallino, The kinetic fragility of Pt-P- and Ni-P-based bulk glass-forming liquids and its thermodynamic and structural signature, Acta Mater. 132 (2017) 118–127.

[38] O. Gross, S.S. Riegler, M. Stolpe, B. Bochtler, R. Busch, I. Gallino, On the high glass–forming ability of Pt–Cu–Ni/Co–P-based liquids, Acta Mater. 141 (2017) 109–119.

[39] G.J. Fan, J.F. Loffler, R.K. Wunderlich, H.J. Fecht, Thermodynamics, enthalpy relaxation and fragility of the bulk metallic glass-forming liquid $Pd_{43}Ni_{10}Cu_{27}P_{20}$, Acta Mater. 52 (2004) 667–674.

[40] M. Yang, X.J. Liu, Y. Wu, H. Wang, X.Z. Wang, Z.P. Lu, Unusual relation between glass-forming ability and thermal stability of high-entropy bulk metallic glasses, Mater. Res. Lett. 6 (2018) 495–500.

[41] N. Nishiyama, A. Inoue, Glass transition behavior and viscous flow working of $Pd_{40}Cu_{30}Ni_{10}P_{20}$ amorphous alloy, Mater. Trans. JIM 40 (1999) 64–71.

[42] C.W. Wang, L.N. Hu, C. Wei, X.D. Hui, Y.Z. Yue, Sub-T_g relaxation patterns in Cu-based metallic glasses far from equilibrium, J. Chem. Phys. 141 (2014) 164507.

[43] O. Kubaschewski, C. Alcock, P. Spencer, Materials Thermochemistry, Pergamon Press, New York, 1993.

[44] H.B. Ke, P. Wen, D.Q. Zhao, W.H. Wang, Correlation between dynamic flow and thermodynamic glass transition in metallic glasses, Appl. Phys. Lett. 96 (2010) 251902.

[45] W. Kauzmann, The nature of the glassy state and the behavior of liquids at low temperatures, Chem. Rev. 43 (1948) 219–256.

[46] Z. Raza, B. Alling, I.A. Abrikosov, Computer simulations of glasses: the potential energy landscape, J. Phys.-Condens. Mat. 27 (2015) 293201.

[47] J. Guo, X.F. Bian, Y. Zhao, S.J. Zhang, T.B. Li, C.D. Wang, Correlation between the fragility of supercooled liquids and thermal expansion in the glassy state for Gd-based glass-forming alloys, J. Phys.-Condens. Mat. 19 (2007) 116103.

[48] M.Q. Jiang, M. Naderi, M. Peterlechner, L.H. Dai, G. Wilde, Thermal expansion accompanying the glass-liquid transition and crystallization. AIP Adv. 5 (1015) 127133.

[49] Q. Hu, X.R. Zeng, M.W. Fu, Characteristic free volumes of bulk metallic glasses: measurement and their correlation with glass-forming ability, J. Appl. Phys. 109 (2011) 053520.

[50] Q. Hu, J.M. Wang, Y.H. Yan, J.Z. Zou, X.R. Zeng, Anomalous thermal expansion in the deep super-cooled liquid region of a Zrcualag bulk metallic glass, Mater. Res. Lett. 6 (2018) 121–129.

[51] T. Hashimoto, T. Numasawa, M. Shino, T. Okada, magnetic refrigeration in the temperature-range from 10K to room – temperature – the ferromagnetic refrigerants, Cryogenics (Guildf) 21 (1981) 647–653.

[52] K.A. Gschneidner, V.K. Pecharsky, A.O. Tsokol, Recent developments in magnetocaloric materials, Rep. Prog. Phys. 68 (2005) 1479–1539.

[53] M.E. Wood, W.H. Potter, General-analysis of magnetic referigeration and its optimization using a new concept – maximization of refrigerant capacity, Cryogenics (Guildf) 25 (1985) 667–683.

[54] V.K. Pecharsky, K.A. Gschneidner, Giant magnetocaloric effect in $Gd_5(Si_2Ge_2)$, Phys. Rev. Lett. 78 (1997) 4494–4497.

[55] V. Provenzano, A.J. Shapiro, R.D. Shull, Reduction of hysteresis losses in the magnetic refrigerant $Gd_5Ge_2Si_2$ by the addition of iron, Nature 429 (2004) 853–857.

[56] Z.G. Zhu, P. Wen, D.P. Wang, R.J. Xue, D.Q. Zhao, W.H. Wang, Characterization of flow units in metallic glass through structural relaxations, J. Appl. Phys. 114 (2013).

[57] W.H. Wang, The nature and properties of amorphous matter, Prog. Phys. 33 (2013) 212–213.

[58] C. Park, M. Saito, Y. Waseda, N. Nishiyama, A. Inoue, Structural study of Pd-based amorphous alloys with wide supercooled liquid region by anomalous X-ray scattering, Mater. Trans. JIM 40 (1999) 491–497.

[59] H.E. Kissinger, Variation of peak temperature with heating rate in differential thermal analysis, J. Res. Natl. Bur. Stand. 57 (1956) 217–221.

[60] L. Liang, X. Hui, C.M. Zhang, G.L. Chen, A Dy-based bulk metallic glass with high thermal stability and excellent magnetocaloric properties, J. Alloys Compd. 463 (2008) 30–33.

[61] R. Busch, J. Schroers, W.H. Wang, Thermodynamics and kinetics of bulk metallic glass, MRS Bull. 32 (2007) 620–623.

[62] R. Busch, The thermophysical properties of bulk metallic glass-forming liquids, JOM 52 (2000) 39–42.

[63] J. Kim, H.S. Oh, J. Kim, C.W. Ryu, G.W. Lee, H.J. Chang, E.S. Park, Utilization of high entropy alloy characteristics in Er–Gd–Y–Al–Co high entropy bulk metallic glass, Acta Mater. 155 (2018) 350–361.

[64] I. Gallino, D. Cangialosi, Z. Evenson, L. Schmitt, S. Hechler, M. Stolpe, B. Ruta, Hierarchical aging pathways and reversible fragile-to-strong transition upon annealing of a metallic glass former, Acta Mater. 144 (2018) 400–410.

[65] Z. Evenson, On the Thermodynamic and Kinetic Properties of Bulk Glass Forming Metallic Systems, Saarland University, 2010.

[66] C.A. Angell, Formation of glasses from liquids and biopolymers, Science 267 (1995) 1924–1935.

[67] J.C. Bendert, A.K. Gangopadhyay, N.A. Mauro, K.F. Kelton, Volume expansion measurements in metallic liquids and their relation to fragility and glass forming ability: an energy landscape interpretation, Phys. Rev. Lett. 109 (2012) 185901.

[68] C.A. Angell, S. Borick, Specific heats C_p, C_v, C_{conf} and energy landscapes of glassforming liquids, J. Non-Cryst. Solids 307 (2002) 393–406.

[69] Z. Wang, P. Wen, L.S. Huo, H.Y. Bai, W.H. Wang, Signature of viscous flow units in apparent elastic regime of metallic glasses, Appl. Phys. Lett. 101 (2012) 121906.

[70] H.B. Yu, W.H. Wang, H.Y. Bai, K. Samwer, The beta-relaxation in metallic glasses, Natl. Sci. Rev. 1 (2014) 429–461.

[71] H.B. Yu, W.H. Wang, H.Y. Bai, Y. Wu, M.W. Chen, Relating activation of shear transformation zones to beta relaxations in metallic glasses, Phys. Rev. B 81 (2010) 220201.

[72] T.F. Middleton, D.J. Wales, Energy landscapes of some model glass formers, Phys. Rev. B 64 (2001) 024205.

[73] Y. Li, Q. Guo, J.A. Kalb, C.V. Thompson, Matching glass-forming ability with the density of the amorphous phase, Science 322 (2008) 1816–1819.

[74] R.J. Xue, L.Z. Zhao, M.X. Pan, B. Zhang, W.H. Wang, Correlation between density of metallic glasses and dynamic fragility of metallic glass-forming liquids, J. Non-Cryst. Solids 425 (2015) 153–157.

[75] S.K. Banerjee, On a generalised approach to 1st and 2nd order magnetic transitions, Phys. Lett. 12 (1964) 16–17.

[76] V. Franco, J.S. Blazquez, A. Conde, Field dependence of the magnetocaloric effect in materials with a second order phase transition: a master curve for the magnetic entropy change, Appl. Phys. Lett. 89 (2006) 222512.

[77] V. Franco, J.S. Blazquez, C.F. Conde, A. Conde, A Finemet-type alloy as a low-cost candidate for high-temperature magnetic refrigeration, Appl. Phys. Lett. 88 (2006) 042505.

[78] A. Arrott, J.E. Noakes, Approximate equation of state for nickel near its critical temperature, Phys. Rev. Lett. 19 (1967) 786–788.

[79] V. Franco, J.S. Blazquez, A. Conde, The influence of co addition on the magnetocaloric effect of nanoperm-type amorphous alloys, J. Appl. Phys. 100 (2006) 064307.

[80] H.F. Belliveau, Y.Y. Yu, H. Srikanth, H.X. Shen, J.F. Sun, M.H. Phan, Improving mechanical and magnetocaloric responses of amorphous melt-extracted Gd-based microwires via nanocrystallization, J. Alloys Compd. 692 (2017) 658–664.

[81] F. Yuan, Q. Li, B.L. Shen, The effect of Fe/Al ratio on the thermal stability and magnetocaloric effect of $Gd_{55}Fe_xAl_{45-x}$ (x=15–35) glassy ribbons, J. Appl. Phys. 111 (2012) 07A937.